



The influence of main channel velocity and water depth changes on the hydrodynamic characteristics of lateral water intake in a tidal channel

Shan Wang ^a, Qilong Bi^b, Wei He ^{a,*} and Jian Zhang^a

^a College of Water Conservancy and Hydropower Engineering, Hohai University, Nanjing 210098, China

^b Flanders Hydraulics Research, Berchenmlei 115, Antwerp 2140, Belgium

*Corresponding author. E-mail: hewei@hhu.edu.cn

 SW, 0000-0002-5788-966X; WH, 0000-0002-3472-2728

ABSTRACT

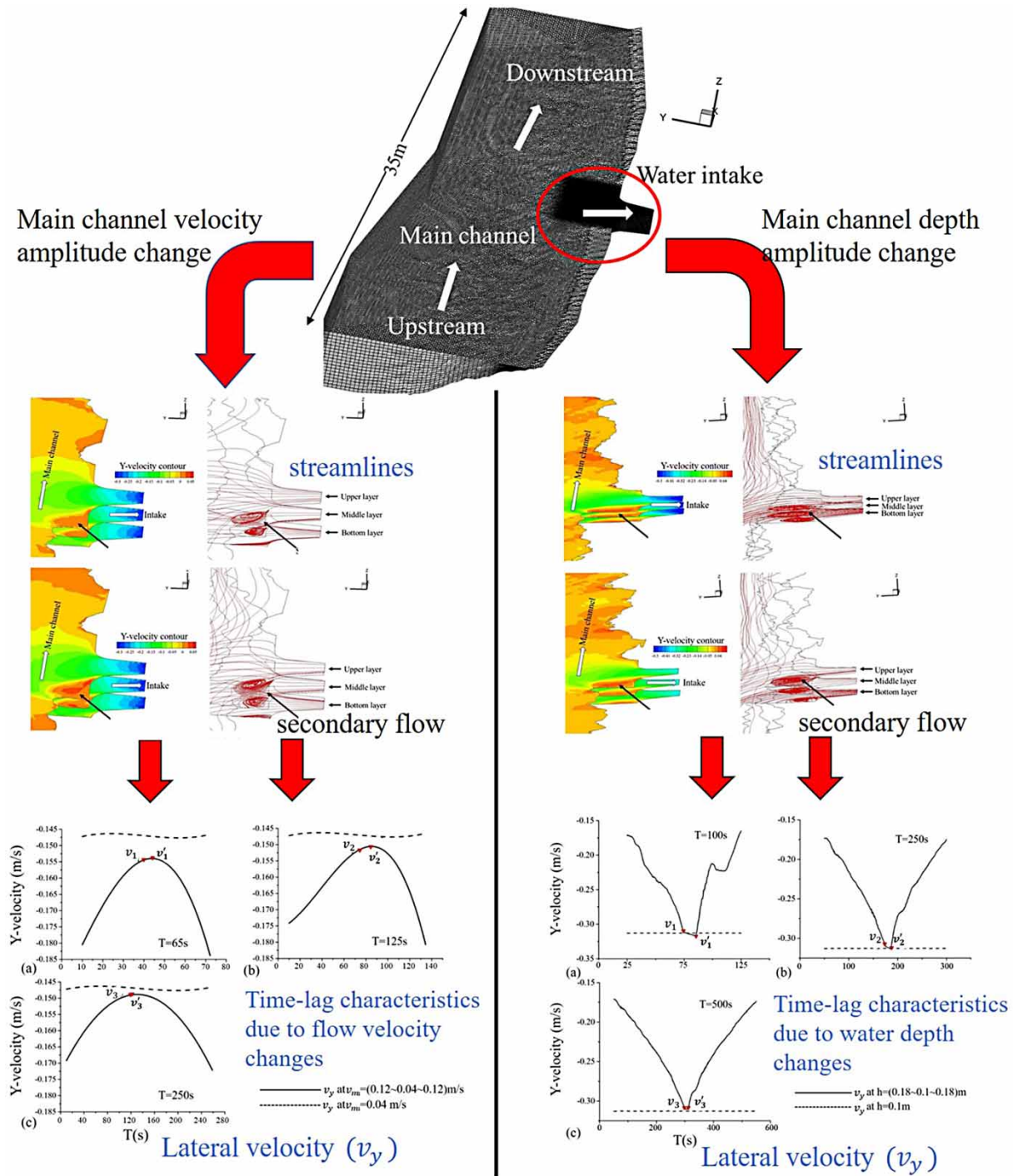
A tidal channel will be affected by the intrusion of seawater, so the current and water depth in the channel will change at every moment. These changes are critical to the hydrodynamic characteristics of water intakes in tidal rivers. This paper establishes a 3D model and validates it through laboratory models, then analyzes the influences of dynamic change of flow velocity and water depth, and the amplitude changes of velocity and water depth on the secondary flow in the water withdrawal process. With the increase of the main flow velocity and the decrease of the water depth, diversion width at the water intake decreases, the peak velocity increases, and the intensity of the secondary flow also increases. With the increase of the velocity of the main channel and the changing rate in water depth, the lag time of the velocity change at the water intake is also longer, and the peak velocity will be greater than the velocity of the constant flow. The influence of the water depth change is greater than that of the main channel velocity change. Combining these four factors, more sand may be washed into the inlet channel under conditions of high flow and low water depth.

Key words: lateral intake, main channel, numerical simulation, TELEMAC-3D, water depth

HIGHLIGHTS

- Hydrodynamic change rule of intake when the water level of main river changes dynamically.
- Hydrodynamic change rule of intake when the velocity of main river changes dynamically.
- Time lag law of hydrodynamic change of water intake with the water level change of main river.
- Time lag law of hydrodynamic change of water intake with the velocity change of main river.
- Optimal water intake combination for tidal channels.

GRAPHICAL ABSTRACT



1. INTRODUCTION

Tidal channels will be affected by seawater intrusion. The flow, water depth, and salinity in the river are changing all the time, and these changes are vital to the construction and operation of a water conservancy project in the river. The water depth of the river channel will rise sharply due to the combined action of the upstream flood and the downstream tide. At the same

time, the flow velocity of the main river channel will also change sharply, which may cause potential harm to the normal work of the water conservancy project in the river (Sassi & Hoitink 2013; Zhang *et al.* 2018; Luo *et al.* 2020).

The hydrodynamic characteristics of lateral water intake projects in tidal channels are quite different from those of non-tidal freshwater channels (El-Jabi *et al.* 1992). Experiments and existing 3D turbulence models are used to study the flow characteristics of diversion flow in an open channel. The results show that the water flow at the lateral water intake has obvious three-dimensional characteristics (Ramamurthy & Satish 1988; Neary & Odgaard 1993; Neary *et al.* 1999). The kinetic energy and hydrostatic pressure of the different sections of the main channel and the lateral channel are different (Yang & Lim 2005; Abderrezzak *et al.* 2011; Asnaashari *et al.* 2016). Compared with the calculated water depth at the lateral entrance, the flow depth along the sidewall is increased, and at the same time, a very obvious secondary flow phenomenon will be observed in the lateral inlet channel. The formation and evolution of the secondary flow are closely related to flow velocity, water depth of the main river, angle of the water entrance, the structure of the water intake, and other factors (Hsu *et al.* 2002; Keshavarzi & Habibi 2005; Keshavarzi *et al.* 2012; Azimi *et al.* 2019). The secondary flow has multiple flow modes such as single vortex and double vortex flow patterns, tornado vortex formation, and air entrainment (Lucas *et al.* 2015). Usually, in a long straight river, the diversion width of the lateral intake is larger at the top and smaller at the bottom. However, in a river with an inclining bank, the inclining bank causes the bottom stream tube width to be greater than at the surface and the strength of the secondary current formed at the entrance of the branch channel is reduced (Ramamurthy *et al.* 2007; Seyedian *et al.* 2014).

The secondary flow will affect the flow velocity and kinetic energy distribution in the downstream and lateral channels (Constantinescu *et al.* 2011), and at the same time, it will also affect the movement process of the sediment at the water intake. If the division width at the bottom is larger, more sediment may move into the water intake channel (Firozjaei *et al.* 2019; Rad *et al.* 2020). To improve the flow pattern, methods such as adding underwater submerged vanes and arranging sand blocking devices are usually adopted. Existing studies are mainly aimed at the constant flow rate of the main river or constant water depth. At present, there are still very few studies on the hydraulic characteristics of the water intake under the dynamic change of the main channel parameters. Under real conditions, the flow of the main river and the water depth always change continuously within a certain range over time, and the feedback process of hydrodynamic changes at the water intake does not occur simultaneously with the changes in the main river flow rate or water depth. The flow condition of the tidal channel will seriously affect the safe and efficient operation of the lateral water intake project. Therefore, the study of the hydrodynamic characteristics of the water intake in the tidal channel is particularly important.

This study will take the Rong river intake project in Zhanjiang City, Guangdong Province, China (this project is close to the estuary) as an example, to establish a laboratory model and combine it with numerical simulation (TELEMAC-3D). The study aims to clarify the hydraulic change mechanism of the lateral intake under the condition of dynamic change of flow parameters in the main channel. First, the effects of water depth and flow velocity changes on the diversion width and the flow velocity distribution in the lateral channel are quantified. Subsequently, the time lag phenomenon of flow parameter change near the water intake was observed, and the law of time lag characteristics changing with the change of main channel flow parameters is qualitatively obtained. Finally, the optimal water intake scheme is derived and the potential sediment movement is predicted. This study will provide a reference for all tidal-affected water intake projects.

2. METHODOLOGY

2.1. Numerical model

2.1.1. The Navier–Stokes equations

TELEMAC-3D is a computational fluid dynamic solver for free surface flows (Hervouet 2007; Le *et al.* 2019). The model solves the 3D Navier–Stokes equations for an incompressible fluid, which consist of two equations: the continuity equation and the momentum equation.

Mass conservation (assuming a constant density of water):

$$\nabla \cdot \mathbf{u} = 0 \quad (1)$$

Momentum equation:

$$\frac{\partial u}{\partial t} + (u \cdot \nabla)u = -\frac{1}{\rho} \nabla p + \frac{1}{\rho} \nabla \cdot (\mu \nabla u) + g \quad (2)$$

where u is the velocity vector, p is the pressure, g is the gravitational acceleration vector, ρ is the fluid density, and μ is the kinematic viscosity.

In large-scale simulations, the model domain usually covers thousands of square kilometres. The horizontal dimension of the water body is far larger than the vertical dimension. Therefore, the diffusion, source terms, and acceleration in the vertical direction can be neglected. In this case, if the pressure at one point only depends on the weight of the column of water above it, the Navier–Stokes equations can be simplified to a hydrostatic version (Hervouet 2007). Given the hydrostatic hypothesis, in Cartesian coordinates, the Navier–Stokes equations are re-written as follows:

Mass conservation:

$$\frac{\partial u_1}{\partial x_1} + \frac{\partial u_2}{\partial x_2} + \frac{\partial u_3}{\partial x_3} = 0 \quad (3)$$

Momentum equation:

$$\frac{\partial u_1}{\partial t} + u_1 \frac{\partial u_1}{\partial x_1} + u_2 \frac{\partial u_1}{\partial x_2} + u_3 \frac{\partial u_1}{\partial x_3} = -\frac{1}{\rho} \left(\frac{\partial p}{\partial x_1} \right) + \mu \left(\frac{\partial^2 u_1}{\partial x_1^2} + \frac{\partial^2 u_1}{\partial x_2^2} + \frac{\partial^2 u_1}{\partial x_3^2} \right) \quad (4)$$

$$\frac{\partial u_2}{\partial t} + u_1 \frac{\partial u_2}{\partial x_1} + u_2 \frac{\partial u_2}{\partial x_2} + u_3 \frac{\partial u_2}{\partial x_3} = -\frac{1}{\rho} \left(\frac{\partial p}{\partial x_2} \right) + \mu \left(\frac{\partial^2 u_2}{\partial x_1^2} + \frac{\partial^2 u_2}{\partial x_2^2} + \frac{\partial^2 u_2}{\partial x_3^2} \right) \quad (5)$$

Pressure:

$$p = p_{\text{atm}} + \rho g (\eta - x_3) + \rho g \int_{x_3}^{\eta} \frac{\Delta \rho}{\rho} dx_3 \quad (6)$$

where x_i is the coordinate in three dimensions and u_i is the component of velocity in the i direction.

2.1.2. Turbulence model

Recently, large eddy simulation (LES) has been proven to improve the accuracy of the existing large-scale river channel numerical model (Khosronejad & Sotiropoulos 2014; Bourgoin *et al.* 2021), which can better capture the local flow regime and the change of bottom shear stress (Kolahdoozan *et al.* 2005). Therefore, this study chooses the LES model as the horizontal turbulence model.

The Smagorinsky model is the first LES turbulence model ever derived (Smagorinsky 1963). If the size of the finite element allows the reproduction of all mechanisms, including the viscous dissipation of very small vortices, then the smallest turbulence scale will naturally appear in the numerical solution. Modeling is performed only in smaller vortex formations, where turbulence is suppressed by the mesh.

The classic Smagorinsky model is computed as:

$$v_t = C_s^2 \Delta^2 \sqrt{2S_{ij}S_{ij}} \quad (7)$$

where v_t is the turbulent viscosity and S_{ij} is the strain rate tensor of the filtered velocities, with:

$$S_{ij} = \frac{1}{2} \left(\frac{\partial u_i}{\partial x_j} + \frac{\partial u_j}{\partial x_i} \right) \quad (8)$$

where C_s is a dimensionless coefficient to be calibrated and Δ is the mesh size derived in 3D from the surface or the volume of an element. In this study, $C_s = 0.1$ (Deardorff 1970; Kolahdoozan *et al.* (2005); Alemi *et al.* 2020).

Based on the assumption that the small scales tend to isotropy, the standard Smagorinsky model relies on the small and isotropic mesh elements. The eddy viscosity is evaluated as the product of a length scale $C_s\Delta$ proportional to the mesh size, and a velocity scale $C_s\Delta|S_{ij}|$ (Bardina *et al.* 1980).

The vertical diffusivity of velocities is then automatically computed by TELEMAC-3D using the selected mixing length model taking or not taking the effects of density into account (Dorfmann & Zenz (2016)). The mixing length model expresses the turbulent viscosity as a function of the mean velocity gradient and the mixing length:

$$v = L_m^2 \sqrt{2D_{ij}D_{ij}} \quad (9)$$

where $D_{ij} = (1/2)((\partial u_i/\partial x_j) + (\partial u_j/\partial x_i))$ and L_m is the length scale of the model.

2.1.3. Model setup

The numerical model will be modeled completely according to the size of the physical model, and the completely open-source computing software TELEMAC-3D will be used for numerical simulation (Figure 1). In TELEMAC modeling systems, the meshes used are based on the sigma coordinate system in the vertical direction (Phillips 1957; Decoene & Gerbeau 2009). This mesh structure is made of prisms. To prepare the mesh for the 3D domain, a 2D mesh made of triangles that

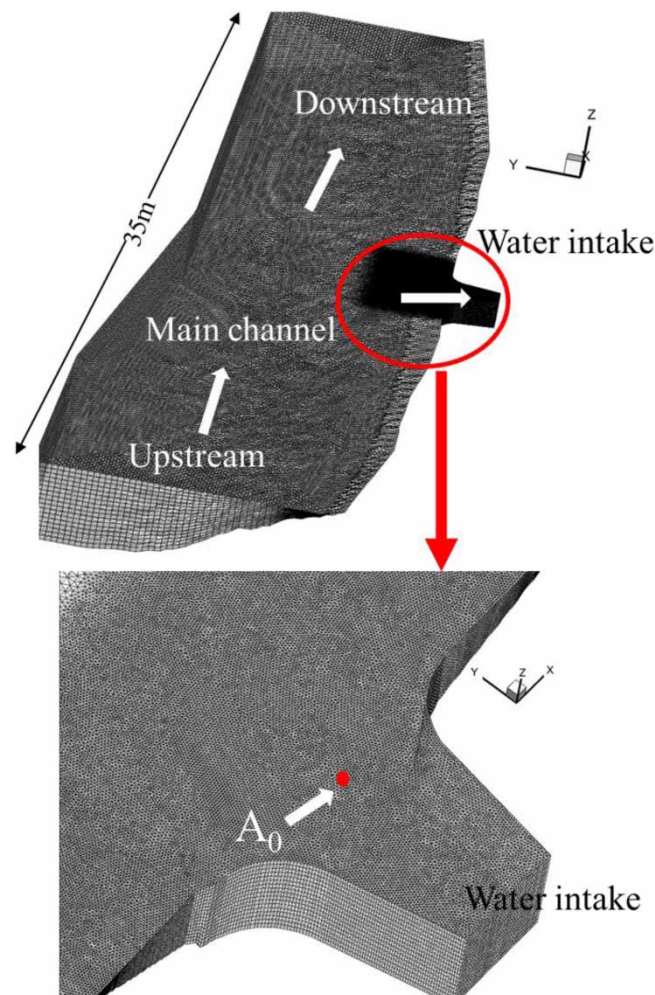


Figure 1 | Illustration of numerical model mesh.

covers the computational domain (the bottom) in a plane is first constructed. The second step consists of replicating this mesh vertically on a number of surfaces called planes. A mapping from (Z_b, Z_s) to $(0,1)$ is used as follows:

$$x_3^* = \frac{x_3 - Z_b}{Z_s - Z_b} = \frac{x_3 - Z_b}{h} \quad (10)$$

where Z_b and Z_s are the bottom elevation and surface elevation, respectively, h being the water depth.

2.1.4. Boundary condition

The upstream uses a flow inlet, the lateral water intake is set as a fixed flow outlet, and the downstream uses a water level outlet. In the simulation working conditions of dynamic flow velocity changes and dynamic water depth changes, the boundary files are given by the Fortran file. The simulation process of water depth change takes into account the influence of tidal flats (Le Hir *et al.* 2000), and at the same time, does not consider the influence of wind, salinity, and temperature. Therefore, there is no difference in the vertical distribution of the inlet flow velocity.

2.1.5. Mesh sensitivity analysis

The v_l from A_1 to A_5 were extracted and used as the monitoring points for mesh independence analysis (monitoring points A_1 to A_{15} are shown in Figure 3(d)). It can be seen from Figure 2 that with increasing mesh density, the difference shown by the numerical simulation results becomes very subtle. When the mesh size is 0.02 and 0.01 m, the velocity values obtained at points A_1 to A_5 are very close. Considering the accuracy of the calculation results and computer performance, the size of the mesh is selected as 0.01 m (Table 1).

2.2. Physical model

The experiment was based on the Rong river water intake project in Guangdong Province, and the original river course was modeled in a laboratory. According to the actual construction measures of the project and the dynamic similarity law, the water depth and hydraulic layout were determined.

The upstream uses multiple water pumps and flow meters to control the flow, as shown in Figure 3(a), and the downstream uses gate weirs to control the water depth. To simulate the effect of tides, the upstream and downstream boundary conditions can be interchanged in the experiment. The water depth gauge is used to measure the water depth, as shown in Figure 3(b). The LGY-III automatic speedometer is used to test the water flow rate, as shown in Figure 3(e). The initial inlet and outlet boundary conditions of the experiment are the same as those of the numerical model. The experimental site is shown in Figure 3(c). The distribution of experimental measuring points A_1 – A_{15} is shown in Figure 3(d), and A_0 will serve as the main speed monitoring point in the subsequent simulation conditions.

The selection of the inlet flow of the river channel in the numerical model all comes from the hydrological report of the actual engineering. In the actual engineering, 125 and 300 m^3/s correspond to the daily upstream flow and the maximum upstream flood flow, respectively. The daily water intake depth and the maximum water intake depth of the water intake are 3 and 5.4 m, respectively. The maximum water depth in the prototype is 23 m. The scale of the model and prototype

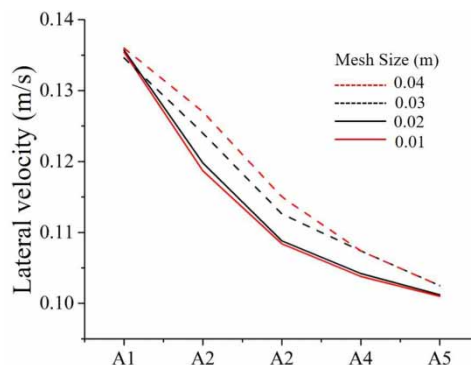


Figure 2 | Mesh independence validation, where v_l means lateral velocity.

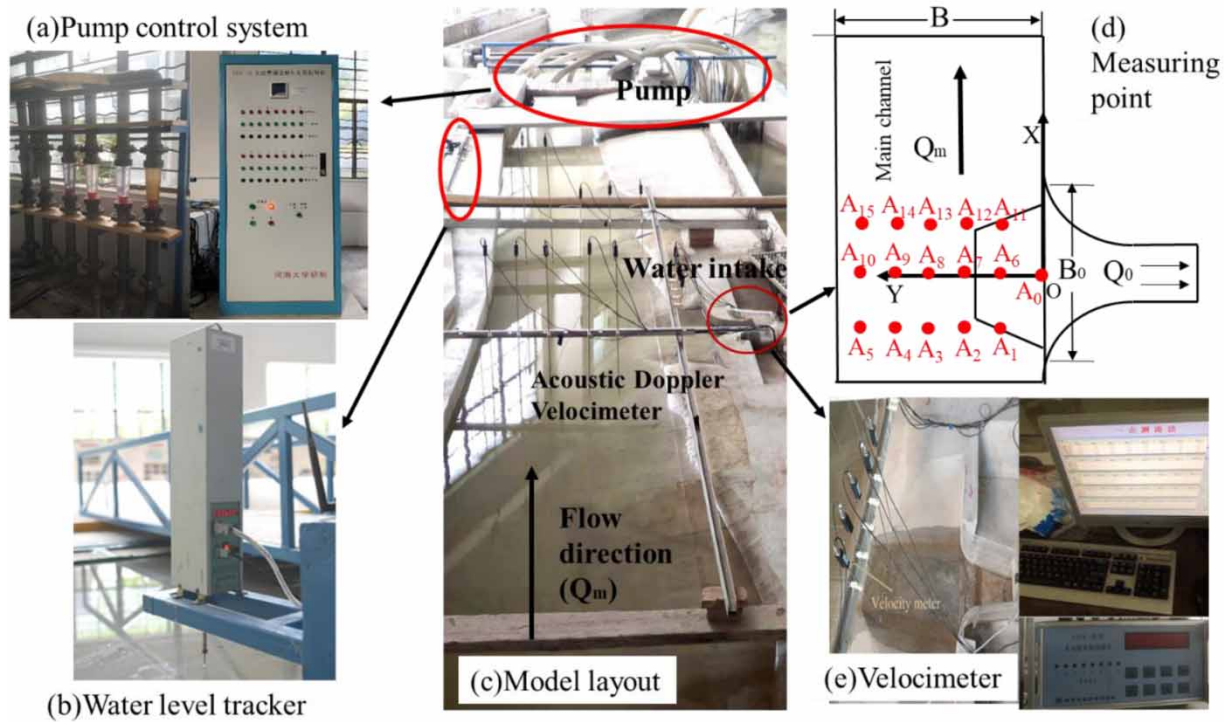


Figure 3 | Experimental device and measuring point distribution: (a) pump control system; (b) water level tracker; (c) model layout; (d) measuring point; and (e) velocimeter system.

Table 1 | Mesh size

| Elements | Average mesh size (m) |
|----------|-----------------------|
| 284,759 | 0.04 |
| 340,307 | 0.03 |
| 371,089 | 0.02 |
| 550,031 | 0.01 |

is 1:30. The length of the model is 17 m, and the maximum water depth of the main channel in the laboratory is 0.78 m. In the laboratory, according to the Froude similarity, 25 and 60 L/s were selected for daily flow and maximum flow, respectively, and water depths of 0.1 and 0.18 m at the water intake were selected as the rated water intake depth and the maximum water intake depth, respectively.

2.3. Model scenarios of numerical simulations

Refer to [Table 2](#) for more details.

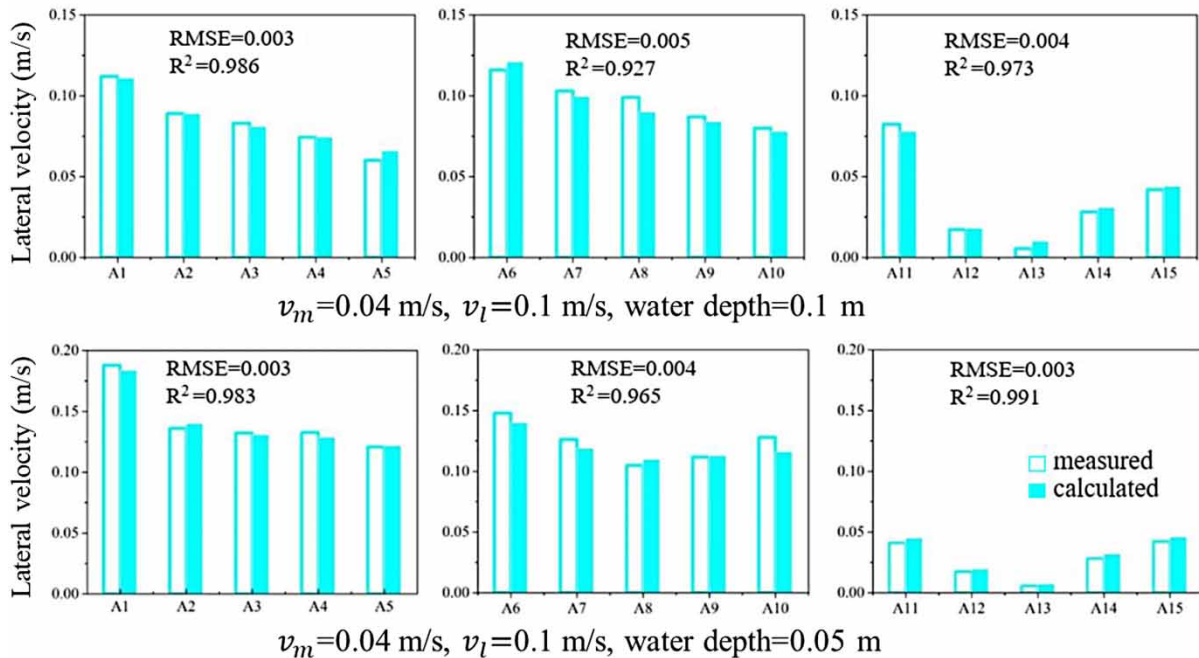
3. RESULTS

3.1. Model validation

The results of the experiment and numerical simulations are shown in [Figure 4](#). The mesh of the numerical model is completely generated according to the layout of the physical model. The root-mean-square error (RMSE) and the coefficient of determination (R^2) are introduced to quantitatively estimate the size of the error between simulation and observation [Moriassi et al. \(2007\)](#). The fitting test shows that the observed value in the physical model test fits well with the calculated value of the numerical simulation, and the numerical model can accurately simulate the flow field.

Table 2 | Introduction of simulated conditions

| Scenario | Description |
|----------|---|
| 3.1 | Model validation |
| 3.2 | Influence of main channel velocity amplitude, 0.04, 0.08, 0.12, and 0.16 m/s, respectively |
| 3.3 | The flow velocity of the main channel uniformly decreased from 0.12 to 0.04 m/s and then increased to 0.12 m/s, which took 60, 125, and 250 s, respectively |
| 3.4 | Influence of water depth, 0.78, 0.74, and 0.7 m, respectively |
| 3.5 | The water depth of the main channel uniformly decreased from 0.78 to 0.7 m and then increased to 0.78 m, which took 100, 250, and 500 s, respectively |

**Figure 4** | Comparison of measured and calculated values of model validation, where v_m is the mainstream velocity and v_l is the lateral withdrawal velocity.

3.2. Influence of main channel velocity amplitude

It can be seen from Figure 5 that although the water intake flow is fixed, the flow velocity distribution in the water intake channel is different. In Figure 5(a), the maximum flow velocity at the inlet of the water intake is about 0.15 m/s. With the increase of the mainstream flow velocity (v_m), the maximum flow velocity at the inlet changes greatly and the flow velocity distribution in the lateral channel becomes more uneven. In Figure 5(d), in the lateral channel, the flow velocity on the side far from the secondary flow center is significantly greater than that on the side close to the secondary flow area, and the maximum flow velocity at the entrance of the water intake can reach 0.25 m/s. The separation zone near the surface is larger than that near the bed. The diversion width also gradually decreases, from 0.18 m in Figure 5(a) at the very beginning to about 0.16 m in Figure 5(d). When v_m is lower, the secondary flow is mainly concentrated in the upper and middle layers. As v_m increases, the secondary flow area in the lower layer is more obvious; meanwhile, it can also be seen from the flow velocity profile that as v_m increases, v_y in the center of the secondary flow will decrease to less than 0.05 m/s.

3.3. The influence of velocity changing ratio of the main channel

Figure 6 shows the average changing process of the mainstream flow velocity (v_m) with time. The variation range of v_m is 0.12–0.04 m/s and then to 0.12 m/s. The speed change rate of v_m in the three graphs gradually decreases. In the figure, v_i

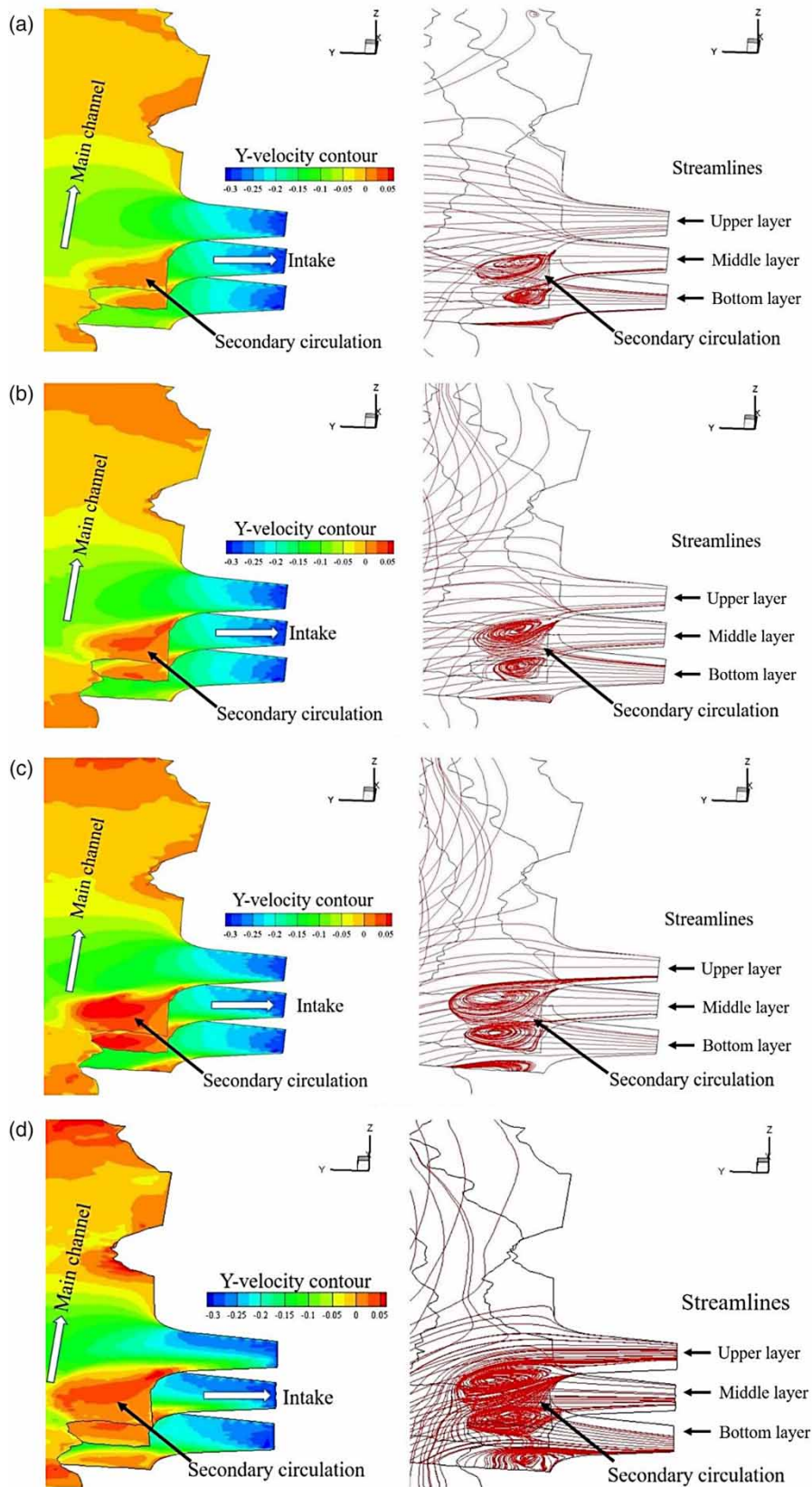


Figure 5 | Lateral velocity contours (left) and flow streamlines (right) under different amplitudes of main channel velocity.

and v'_i do not overlap, that is to say, the velocity at the middle time is not the inflection point of the velocity during the change, and the value of v'_i is always slightly smaller than v_i . Under the steady flow of $v_m = 0.18$ m/s, v_y at this time is about 0.148 m/s. During the dynamic change of v_m , the value of v_y at any time is greater than 0.148 m/s. In the case of rapid changes in the flow velocity of the main channel such as in Figure 6(a), whether it is v_i or v'_i , its value is far from the dotted line. As the speed change rate of v_m slows down, in the middle of the change process, v_i and v'_i tend to overlap, and their values will be closer to v_y under a fixed flow state.

3.4. Influence of main channel water depth

The influence of the water depth of the river channel on the secondary flow is obvious. In Figure 7(a), the diversion width is the largest, and the secondary flow is the smallest, mainly concentrated in the middle and upper layers. The maximum velocity in the y-direction is about 0.32 m/s. As the water depth decreases, as shown in Figure 7(b) and 7(c), the secondary flow at the bottom layer will become stronger. The flow velocity in the lateral water intake channel is significantly accelerated. From the velocity contour of Figure 7(c), it can be seen that the velocity distribution of the upper, middle, and lower layers is the same, and the maximum velocity in the y-direction can reach 0.45 m/s. Observed from the streamline diagram, the structure of the secondary flow is slightly different, which should be caused by the trapezoidal structure here.

3.5. The influence of water depth changing ratio in the main channel

In the three pictures of Figure 8, the dotted line represents v_y at A_0 when $h = 0.1$ m. It should be stable with time. The rate of water depth change shown in the three pictures is gradually slowing down, and the velocity value at the lowest water depth ($h = 0.1$ m) is not the velocity inflection point value during the entire change process. When the water depth changes to the lowest point, the flow velocity at A_0 is still slightly lower than the flow velocity under the stable water depth. In the process of rapid water depth changes such as Figure 8(a), v'_1 appears below the dotted line, that is, the value of v'_1 at this time has exceeded the velocity under the stable water depth. As the rate of change slows, v_i and v'_i gradually converge, and both will be above the dotted line. The change is more like a V-shaped curve, which means the velocity value at A_0 should be symmetric during the change of the water depth from large to small and then to large. This pattern cannot be seen when the water depth changes rapidly. It can be deduced that as the water depth changes slowly enough, v_i and v'_i should be the coincident point, and the value of velocity should be equal to the value when the water depth is stable at 0.1 m.

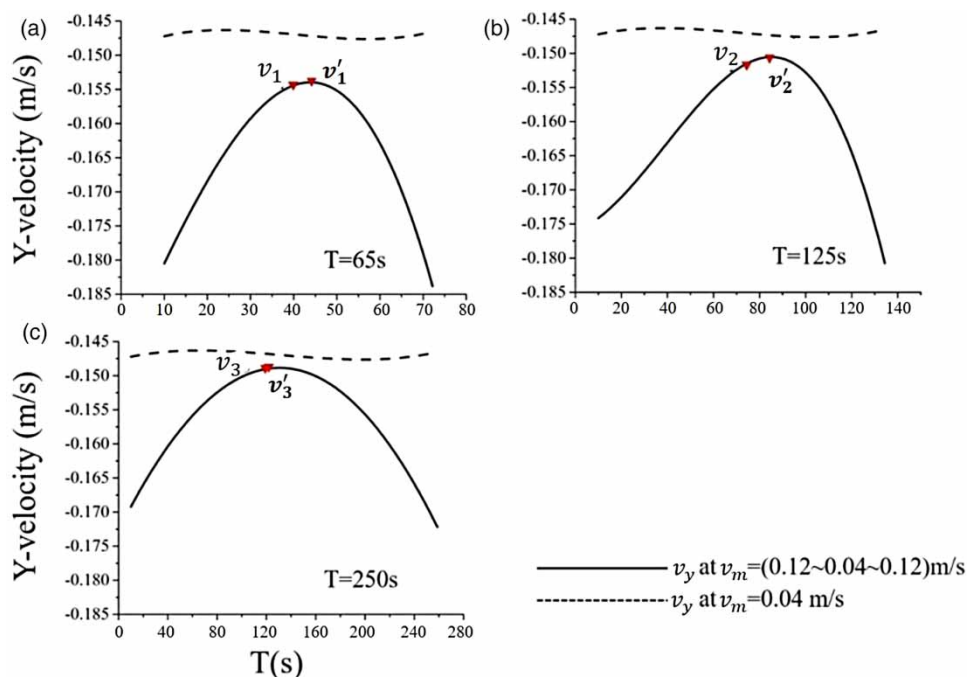


Figure 6 | The curve of uniform change of velocity with time in y-direction (v_y) at A_0 , where v_i means the v_y at the middle time, and v'_i means v_y at the inflection point in the process of change.

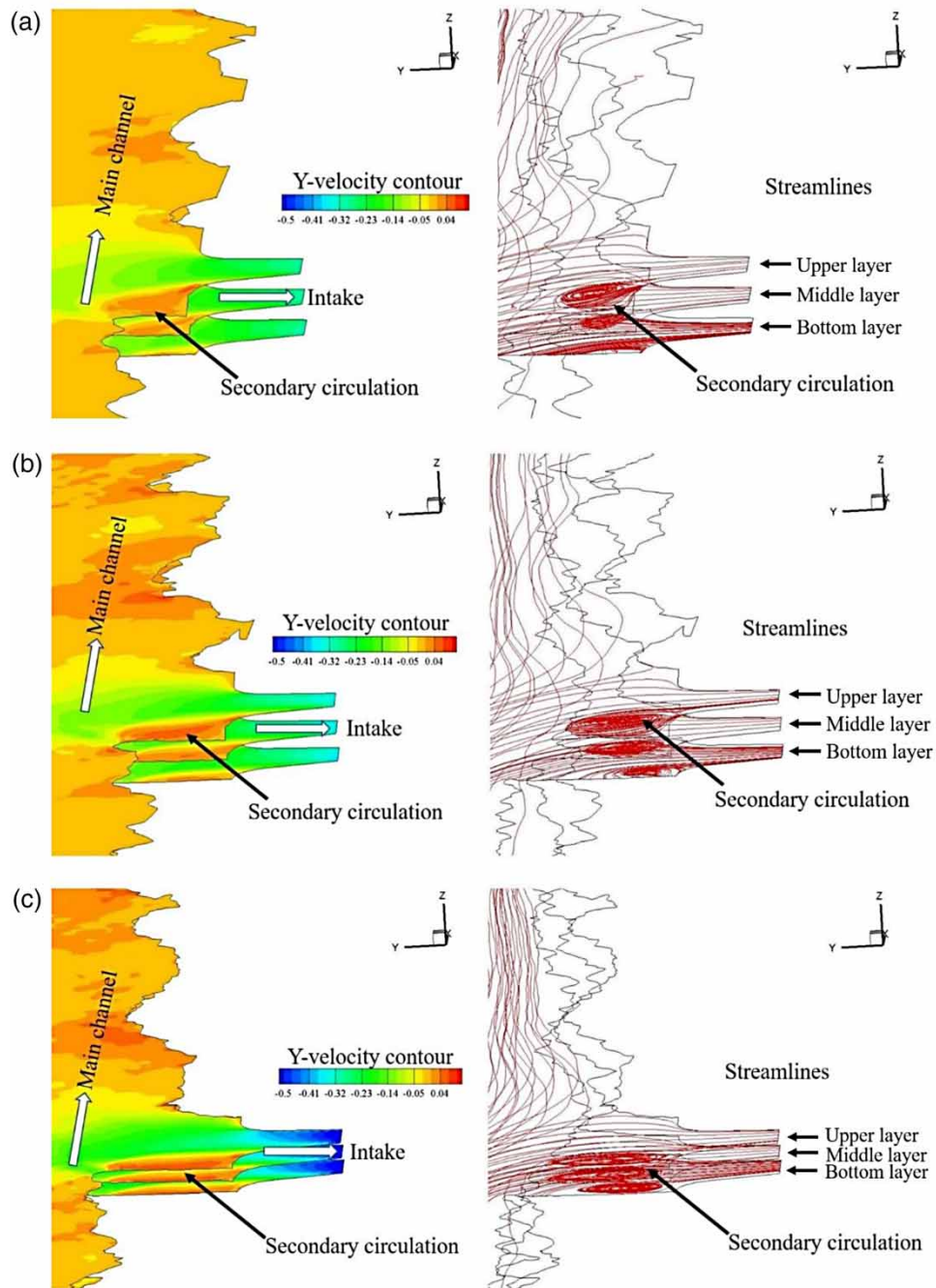


Figure 7 | Lateral velocity contours (left) and flow streamlines (right) under different amplitudes of main channel water depth.

4. DISCUSSION

The flow velocity amplitude of the main channel and the water depth near the lateral entrance have a significant impact on the secondary flow of the intake. As shown in Figure 9(a), when the flow velocity of the main channel is low or the water depth is high, the diversion width of the bottom layer is usually larger than that of the top layer, and the variation trend of diversion width in the upper, middle, and lower layers is the same. The inflection point of the main river flow velocity and water depth change is not the inflection point of the intake flow velocity. Generally, the change of the intake flow velocity has a certain hysteresis. As shown in Figure 9(b), the development of this hysteresis is affected by the change of the main river

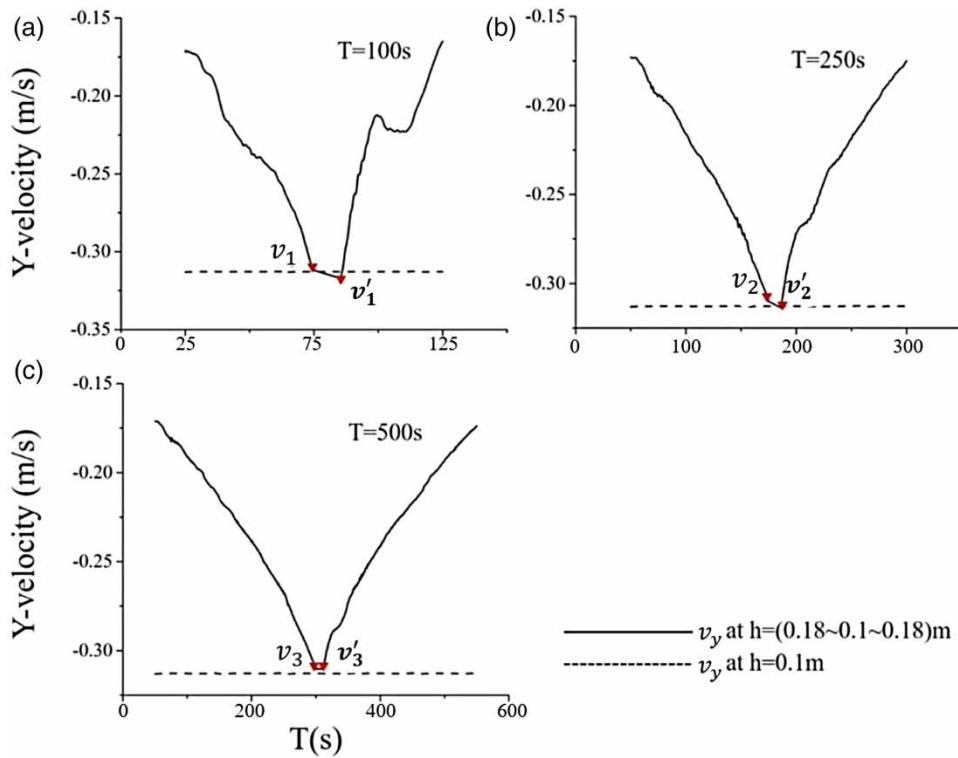


Figure 8 | The curve of uniform change of velocity with time in the y-direction (v_y) at A_0 , where v_i means the v_y at the middle time, and v'_i means v_y at the inflection point in the process of change.

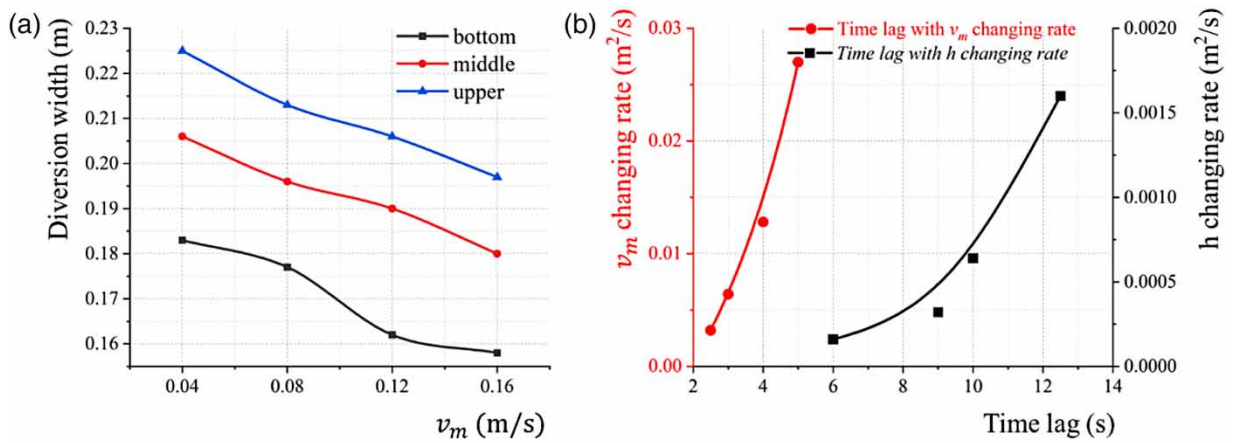


Figure 9 | (a) The change of diversion width with the main flow velocity and (b) the relationship between y-direction (v_y) lag time and the main parameters.

flow velocity and the speed of the water depth and has some specific laws. The influence of the changing rate of h on v_y lag is stronger than that of changing rate of v_m . Generally, the faster the change, the more unstable the flow in the lateral channel. For example, the water depth drops from 0.8 to 0.7 m. If this process is fast enough, when the water depth drops to $h = 0.7$ m, the flow velocity at the water intake will be greater than the flow velocity when the water depth is constant at 0.7 m. This must be taken into account in actual situations because this phenomenon will be a safety hazard (Unami *et al.* 1997). If only the flow velocity under a constant flow state is used as a reference for actual engineering design, there may be a different effect of water extraction from the design expectations.

With the increase of the flow velocity of the main river or the decrease of the water depth, the width of the bottom flow will become smaller, the local flow velocity in the y -direction will increase, and the influence range of the secondary flow will also expand (Huang *et al.* 2002). Considering the movement of sediment, if the excessive flow velocity exceeds the starting flow velocity of the bottom sediment, the bottom sand will rush into the water intake. In contrast, the flow velocity at the center of the secondary flow is lower. If the range of the secondary flow is larger, it may cause more siltation at the inlet, which is very unfavorable for the entire water intake process. Considering that this study is based on actual engineering, the water intake flow at the intake remains unchanged throughout the year. Therefore, the secondary flow at the intake is completely affected by the main flow velocity and water depth.

For this study, the complex secondary flow regime at the water intake and the flow regime in the side channels can be more accurately captured by using the LES model (Bourgoin *et al.* 2021). Of course, this study also has certain limitations. In the actual river channel, the tide will not only affect the water depth and flow velocity of the main channel, but also the seawater intrusion will cause the flow velocity stratification phenomenon in the main channel (He *et al.* 2021; Zhao *et al.* 2022), and then affect the hydrodynamic characteristics of the water intake (Kuijper & Van Rijn 2011; Krvavica & Ružić 2020). In this paper, the influence of salinity was not considered in the process of physical experiment and numerical simulation. Meanwhile, other factors such as wave, temperature, and wind force may also indirectly affect the hydraulic characteristics of the water intake. The next steps are as follows. First, improve the existing numerical model and consider the effects of wind, salinity, and waves in the numerical simulation. Secondly, study the law of sediment and pollutant transport in the river during the water intake process, and promote more accurate and practical models in actual projects.

5. CONCLUSION

Ensuring the efficiency and safety of lateral water intakes in tidal rivers is of great significance to the entire water intake project. This study uses a combination of physical experiments and numerical simulation to analyze the influences of mainstream velocity amplitude, mainstream velocity speed change rate, the water depth amplitude, and the water depth speed change rate on the flow pattern of the water intake. The following conclusions are drawn:

- (1) As the main flow velocity increases, the range of the secondary flow gradually becomes larger, the difference in the vertical distribution becomes more obvious, and the shunt width becomes narrower. In this study, the diversion width is reduced from the initial 0.18–0.16 m. As the water depth decreases, the secondary flow range gradually expands, and the distribution of the upper and middle layers is more similar. The peak velocity in the lateral channel increases significantly, which is about 0.45 m/s in this study. At the lowest water depth, the simulation results show that the diversion width of the bottom layer will decrease significantly, and is reduced from the initial 0.16 to 0.14 m. The decreasing diversion width will result in a more uneven flow velocity distribution at the lateral intake.
- (2) Depending on the changing rate of v_m , v_y will have a lag time of up to 5 s. The lag time increases with the rate of velocity change in the main channel. The peak velocity of v_y with non-constant flow will be slightly lower than that of v_y with constant flow. Depending on the changing rate of water depth in the main channel, the v_y will have a maximum lag time of 12.5 s. The lag time increases with the rate of water depth change in the main channel. If the water depth changes too fast, the peak value of v_y will be greater than the flow velocity under the constant water depth in a short period. By comparing the influence of the two factors on the lag time, the effect of water depth change rate is more prominent.
- (3) When the main flow velocity or water depth changes rapidly, extreme working conditions should be considered. For example, in the dynamic change process of the water depth in this study, if sediment erosion and siltation are considered, in extreme cases, once the flow velocity in the y -direction of the water intake is greater than the initial movement velocity of the sediment, some of the sediment may be washed into the lateral channel. At the same time, as the range of the secondary flow increases, more sediment may be deposited at the entrance. Therefore, the slower flow velocity and deeper water depth of the main river are more favorable water intake conditions. Also in actual projects, a certain threshold should be set according to the designed water intake conditions, or measures such as submerged vanes (Firozjaei *et al.* 2019) and sand traps should be taken to improve the flow regime.

This qualitative law of hysteresis of hydraulic parameters is proposed for the first time in this study. When designing the water intake flow, the adverse effect of this hysteresis phenomenon on the water intake process has to be considered. Follow-up research can only be carried out after clarifying the hydraulic mechanism of the water intake, including sediment

transport, pollutant transport, etc. This study should provide a reference for all water intake projects affected by tidal channels.

FUNDING

This study was supported by the National Natural Science Foundation of China (51879087, 51909070), the Natural Science Foundation of Jiangsu Province (BK20190488, BK20180505), and the fifth '333 Project' of Jiangsu Province (BRA2018061).

DATA AVAILABILITY STATEMENT

Data cannot be made publicly available; readers should contact the corresponding author for details.

CONFLICT OF INTEREST

The authors declare there is no conflict.

REFERENCES

- Abderrezzak, K. E. K., Lewicki, L., Paquier, A., Rivière, N. & Travin, G. 2011 Division of critical flow at the three-branch open-channel intersection. *Journal of Hydraulic Research* **49** (2), 231–238. <https://doi.org/10.1080/00221686.2011.558174>.
- Alemi, M., Pégó, J. P. & Maia, R. 2020 Characterization of the turbulent flow around complex geometries using wall-modeled large eddy simulation and immersed boundary method. *International Journal of Civil Engineering* **18**, 279–291. <https://doi.org/10.1007/s40999-019-00472-9>.
- Asnaashari, A., Merufinia, E., Aminnejad, B. & Khoshtinat, S. 2016 Numerical investigation of the effect of the turbulence in predicting flow velocity distribution, turbulence kinetic energy and hydrostatic pressure on the lateral intakes. *Journal of Vibroengineering* **18** (4), 2429–2436. <https://doi.org/10.21595/jve.2015.15924>.
- Azimi, H., Shabanlou, S. & Kardar, S. 2019 Flow field within rectangular lateral intakes in the subcritical flow regimes. *Modeling Earth Systems and Environment* **5**, 421–430. <https://doi.org/10.1007/s40808-018-0548-4>.
- Bardina, J., Ferziger, J. H. & Reynolds, W. C. 1980 Improved subgrid models for large eddy simulation. In: *13th Fluid and Plasma Dynamics Conference*, American Institute of Aeronautics and Astronautics, 14–16 July, Snowmass, CO, USA. <https://doi.org/10.2514/6.1980-1357>.
- Bourgoin, A., Guillou, S. S., Thiébot, J. & Ata, R. 2021 Use of large-eddy simulation for the bed shear stress estimation over a dune. *International Journal of Sediment Research* **36** (6), 687–695. <https://doi.org/10.1016/j.ijsrc.2019.10.002>.
- Constantinescu, G., Miyawaki, S., Rhoads, B., Sukhodolov, A. & Kirkil, G. 2011 Structure of turbulent flow at a river confluence with momentum and velocity ratios close to 1: insight provided by an eddy-resolving numerical simulation. *Water Resources Research* **47**, W05507. <https://doi.org/10.1029/2010WR010018>.
- Deardorff, J. W. 1970 A numerical study of three-dimensional turbulent channel flow at large Reynolds numbers. *Journal of Fluid Mechanics* **41**, 453–480. <https://doi.org/10.1017/S0022112070000691>.
- Decoene, A. & Gerbeau, J. F. 2009 Sigma transformation and ALE formulation for three-dimensional free surface flows. *International Journal for Numerical Methods in Fluids* **59**, 357–386. <https://doi.org/10.1002/flid.1816>.
- Dorfmann, C. & Zenz, G. 2016 The depth-averaged Mixing Length turbulence model for Telemac-2D. In: *Proceedings of the XXIIIrd TELEMAC-MASCARET User Conference 2016, 11 to 13 October 2016, Paris, France* (S. Bourban, ed.), HR Wallingford, Wallingford, UK, pp. 163–168.
- El-Jabi, N., Wakim, G. & Sarraf, S. 1992 Stage-discharge relationship in tidal rivers. *Journal of Waterway, Port, Coastal, and Ocean Engineering* **118**, 166–174. [https://doi.org/10.1061/\(ASCE\)0733-950X\(1992\)118:2\(166\)](https://doi.org/10.1061/(ASCE)0733-950X(1992)118:2(166)).
- Firozjaei, M. R., Neyshabouri, S. A. A. S., Sola, S. A. & Mohajeri, S. H. 2019 Numerical simulation on the performance improvement of a lateral intake using submerged vanes. *Iranian Journal of Science and Technology, Transactions of Civil Engineering* **43**, 167–177. <https://doi.org/10.1007/s40996-018-0126-z>.
- He, W., Jiang, A., Zhang, J., Xu, H., Xiao, Y., Chen, S. & Yu, X. 2021 Hydrodynamic characteristics of lateral withdrawal in a tidal river channel with saltwater intrusion. *Ocean Engineering* **228**, 108905. <https://doi.org/10.1016/j.oceaneng.2021.108905>.
- Hervouet, J.-M. 2007 *Hydrodynamics of Free Surface Flows: Modelling with the Finite Element Method*. John Wiley & Sons, Chichester, UK.
- Hsu, C. C., Tang, C. J., Lee, W. J. & Shieh, M. Y. 2002 Subcritical 90° equal-width open-channel dividing flow. *Journal of Hydraulic Engineering* **128**, 716–720. [https://doi.org/10.1061/\(ASCE\)0733-9429\(2002\)128:7\(716\)](https://doi.org/10.1061/(ASCE)0733-9429(2002)128:7(716)).
- Huang, J. C., Weber, L. J. & Lai, Y. G. 2002 Three-dimensional numerical study of flows in open-channel junctions. *Journal of Hydraulic Engineering* **128**, 268–280. [https://doi.org/10.1061/\(ASCE\)0733-9429\(2002\)128:3\(268\)](https://doi.org/10.1061/(ASCE)0733-9429(2002)128:3(268)).
- Keshavarzi, A. & Habibi, L. 2005 Optimizing water intake angle by flow separation analysis. *Irrigation and Drainage* **54**, 543–552. <https://doi.org/10.1002/ird.207>.
- Keshavarzi, A., Moghadam, M. K. & Ball, J. E. 2012 Optimising round-edged entrance of 55° river water intake. *Proceedings of the Institution of Civil Engineers – Water Management* **165** (1), 9–19. <https://doi.org/10.1680/wama.2012.165.1.9>.

- Khosronejad, A. & Sotiropoulos, F. 2014 Numerical simulation of sand waves in a turbulent open channel flow. *Journal of Fluid Mechanics* **753**, 150–216. <https://doi.org/10.1017/jfm.2014.335>.
- Kolahdoozan, M., Taher-Shamsi, A., Sadeghi-Bagheneh, M. & Mohamadian, A. 2005 Two-dimensional model for lateral intake flows. *Proceedings of the Institution of Civil Engineers – Water Management* **158**, 141–150. <https://doi.org/10.1680/wama.2005.158.4.141>.
- Krvavica, N. & Ružić, I. 2020 Assessment of sea-level rise impacts on salt-wedge intrusion in idealized and Neretva River Estuary. *Estuarine, Coastal and Shelf Science* **234**, 106638. <https://doi.org/10.1016/j.ecss.2020.106638>.
- Kuijper, K. & Van Rijn, L. C. 2011 Analytical and numerical analysis of tides and salinities in estuaries; part II: salinity distributions in prismatic and convergent tidal channels. *Ocean Dynamics* **61**, 1743–1765. <https://doi.org/10.1007/s10236-011-0454-z>.
- Le, T. B., Khosronejad, A., Sotiropoulos, F., Bartelt, N., Woldeamlak, S. & Dewall, P. 2019 Large-eddy simulation of the Mississippi River under base-flow condition: hydrodynamics of a natural diffuence-confluence region. *Journal of Hydraulic Research* **57** (6), 836–851. <https://doi.org/10.1080/00221686.2018.1534282>.
- Le Hir, P., Roberts, W., Cazaillet, O., Christie, M., Bassoullet, P. & Bacher, C. 2000 Characterization of intertidal flat hydrodynamics. *Continental Shelf Research* **20**, 1433–1459. [https://doi.org/10.1016/S0278-4343\(00\)00031-5](https://doi.org/10.1016/S0278-4343(00)00031-5).
- Lucas, J., Lutz, N., Lais, A., Hager, W. H. & Boes, R. M. 2015 Side-channel flow: physical model studies. *Journal of Hydraulic Engineering* **141**, 05015003. [https://doi.org/10.1061/\(ASCE\)HY.1943-7900.0001029](https://doi.org/10.1061/(ASCE)HY.1943-7900.0001029).
- Luo, X. Y., Zhang, W., Chen, S. J., Feng, X., Ji, X. M. & Xu, Y. W. 2020 Evolution of reversal of the lowest low waters in a tidal river network. *Journal of Hydrology* **585**, 124701. <https://doi.org/10.1016/j.jhydrol.2020.124701>.
- Moriasi, D. N., Arnold, J. G., Van Liew, M. W., Bingner, R. L., Harmel, R. D. & Veith, T. L. 2007 Model evaluation guidelines for systematic quantification of accuracy in watershed simulations. *Transactions of the ASABE* **50** (3), 885–900. <http://dx.doi.org/10.13031/2013.23153>.
- Neary, V. S. & Odgaard, A. J. 1993 Three-dimensional flow structure at open-channel diversions. *Journal of Hydraulic Engineering* **119**, 1223–1230. [https://doi.org/10.1061/\(ASCE\)0733-9429\(1993\)119:11\(1223\)](https://doi.org/10.1061/(ASCE)0733-9429(1993)119:11(1223)).
- Neary, V. S., Sotiropoulos, F. & Odgaard, A. J. 1999 Three-dimensional numerical model of lateral-intake inflows. *Journal of Hydraulic Engineering* **125**, 126–140. [https://doi.org/10.1061/\(ASCE\)0733-9429\(1999\)125:2\(126\)](https://doi.org/10.1061/(ASCE)0733-9429(1999)125:2(126)).
- Phillips, N. A. 1957 A coordinate system having some special advantages for numerical forecasting. *Journal of Meteorology* **14** (2), 184–185. [https://doi.org/10.1175/1520-0469\(1957\)014<0184:ACSHSS>2.0.CO;2](https://doi.org/10.1175/1520-0469(1957)014<0184:ACSHSS>2.0.CO;2).
- Rad, P. H., Kamanbedast, A., Heidarnejad, M., Masjedi, A. & Hasonizadeh, H. 2020 The effect of convergence and divergence on flow pattern and sediment transport in lateral intakes using physical and numerical models. *Ain Shams Engineering Journal* **11** (2), 445–454. <https://doi.org/10.1016/j.asej.2019.08.016>.
- Ramamurthy, A. S. & Satish, M. G. 1988 Division of flow in short open channel branches. *Journal of Hydraulic Engineering* **114**, 428–438. [https://doi.org/10.1061/\(ASCE\)0733-9429\(1988\)114:4\(428\)](https://doi.org/10.1061/(ASCE)0733-9429(1988)114:4(428)).
- Ramamurthy, A. S., Qu, J. & Vo, D. 2007 Numerical and experimental study of dividing open-channel flows. *Journal of Hydraulic Engineering* **133** (10), 1135–1144. [https://doi.org/10.1061/\(ASCE\)0733-9429\(2007\)133:10\(1135\)](https://doi.org/10.1061/(ASCE)0733-9429(2007)133:10(1135)).
- Sassi, M. G. & Hoitink, A. J. F. 2013 River flow controls on tides and tide-mean water level profiles in a tidal freshwater river. *Journal of Geophysical Research – Oceans* **118**, 4139–4151. <https://doi.org/10.1002/jgrc.20297>.
- Seyedian, S. M., Bajestan, M. S. & Farasati, M. 2014 Effect of bank slope on the flow patterns in river intakes. *Journal of Hydrodynamics* **26**, 482–492. [https://doi.org/10.1016/S1001-6058\(14\)60055-X](https://doi.org/10.1016/S1001-6058(14)60055-X).
- Smagorinsky, J. 1963 General circulation experiments with the primitive equations. *Monthly Weather Review* **91** (3), 99–164. [https://doi.org/10.1175/1520-0493\(1963\)091<0099:GCEWTP>2.3.CO;2](https://doi.org/10.1175/1520-0493(1963)091<0099:GCEWTP>2.3.CO;2).
- Unami, K., Kawachi, T., Yangyuoru, M. & Hasegawa, T. 1997 Reliability of steady surface profile in an irrigation canal. *Journal of Irrigation and Drainage Engineering* **123** (1), 13–18. [https://doi.org/10.1061/\(ASCE\)0733-9437\(1997\)123:1\(13\)](https://doi.org/10.1061/(ASCE)0733-9437(1997)123:1(13)).
- Yang, S. Q. & Lim, S. Y. 2005 Boundary shear stress distributions in trapezoidal channels. *Journal of Hydraulic Research* **43**, 98–102. <https://doi.org/10.1080/00221680509500114>.
- Zhang, X. Q., Bao, W. M., Liang, W. Q. & Shen, D. D. 2018 A variable parameter bidirectional stage routing model for tidal rivers with lateral inflow. *Journal of Hydrology* **564**, 1036–1047. <https://doi.org/10.1016/j.jhydrol.2018.07.065>.
- Zhao, W. L., Zhang, J., He, W., Shi, L. & Chen, X. Y. 2022 Effects of diversion wall on the hydrodynamics and withdrawal sediment of a lateral intake. *Water Resources Management* **36**, 1057–1073. <https://doi.org/10.1007/s11269-022-03073-9>.

First received 18 July 2022; accepted in revised form 10 February 2023. Available online 20 February 2023